

Constrained path Monte Carlo method for fermion ground states

Shiwei Zhang*

Center for Nonlinear Studies and Theoretical Division, Los Alamos National Laboratory, Los Alamos, New Mexico 87545
and Department of Physics, The Ohio State University, Columbus, Ohio 43210

J. Carlson and J. E. Gubernatis

Theoretical Division, Los Alamos National Laboratory, Los Alamos, New Mexico 87545

(Received 8 July 1996)

We describe and discuss a recently proposed quantum Monte Carlo algorithm to compute the ground-state properties of various systems of interacting fermions. In this method, the ground state is projected from an initial wave function by a branching random walk in an overcomplete basis of Slater determinants. By constraining the determinants according to a trial wave function $|\psi_T\rangle$, we remove the exponential decay of signal-to-noise ratio characteristic of the sign problem. The method is variational and is exact if $|\psi_T\rangle$ is exact. We illustrate the method by describing in detail its implementation for the two-dimensional one-band Hubbard model. We show results for lattice sizes up to 16×16 and for various electron fillings and interaction strengths. With simple single-determinant wave functions as $|\psi_T\rangle$, the method yields accurate (often to within a few percent) estimates of the ground-state energy as well as correlation functions, such as those for electron pairing. We conclude by discussing possible extensions of the algorithm. [S0163-1829(97)08611-6]

I. INTRODUCTION

We describe a ground-state quantum Monte Carlo (QMC) algorithm that removes the *exponential* scaling of computation time with system size which is characteristic of the infamous fermion “sign problem”^{1,2} in QMC simulations.³⁻⁵ Here we discuss the general concepts of the algorithm, which is approximate, and then describe details for its implementation using the Hubbard model as an example. The test results we present will show that the algorithm makes it possible to compute, in times scaling *algebraically* with system size, general ground-state properties, such as superconducting pairing correlation functions. A brief description of the basic algorithm and some of the results on the Hubbard model were published earlier.⁶ The algorithm, as it will be detailed here, can also be directly applied to study many other lattice models of electron correlations, such as the extended Hubbard model, the Anderson lattice model, etc., where computer simulations with existing QMC algorithms are often difficult and sometimes impossible. Application of the method to more general problem classes, such as atoms, molecules, and nuclei, is currently under study.

The algorithm, called the constrained path Monte Carlo (CPMC) method, has two main ingredients: The *first* is casting the projection of the ground state from an arbitrary initial state as importance-sampled branching random walks in a space of Slater determinants. The *second* ingredient is constraining the paths of the random walks so that any Slater determinant generated maintains a positive overlap with a known trial wave function $|\psi_T\rangle$. This ingredient is used only to deal with the sign problem.

The first of the two ingredients is an exact procedure. As we will illustrate, it combines important advantages of two existing methods, the Green’s function Monte Carlo (GFMC) (Refs. 3, 7, and 8) and the auxiliary-field quantum Monte Carlo (AFQMC) (Refs. 9–12) methods. For example,

our method shares with the latter the ease of computing expectation values of certain correlation functions, which are crucial to probe physical properties but which are often hard to compute accurately by the standard GFMC methods. On the other hand, it shares the GFMC concept of importance sampling with a trial wave function $|\psi_T\rangle$, which greatly improves its efficiency over the AFQMC method. In addition, the realization of the projection by open-ended random walks along the imaginary-time direction makes it practical and easy to implement the second ingredient, the constrained path approximation, and hence to eliminate the exponential scaling due to the sign problem.

The constrained path approximation ensures that the Monte Carlo representation of the projected ground state has *no* asymptotic signal-to-noise ratio decay in imaginary time. The resulting method is variational, with the computed ground-state energy being an upper bound, and becomes exact if $|\psi_T\rangle$ is exact. The constrained-path approximation builds upon the positive projection technique of Fahy and Hamann,¹³ but can also be viewed as a generalization of the fixed-node¹⁴⁻¹⁶ approximation in the GFMC method. Because of the different bases in which the approximations are applied, the effect of the constrained path approximation is expected to be *different* from that of the fixed-node approximation.

In Sec. II, we will summarize the Green’s function Monte Carlo and the auxiliary-field quantum Monte Carlo methods for ground-state calculations. Here, we will establish the necessary concepts and formalisms from these existing approaches that are integral parts of our method. In Sec. III, we describe the CPMC method in general terms, focusing on the concept of the importance-sampled random walks in Slater-determinant space, the nature and consequences of the constrained path approximation, and the computation of expectation values. Implementation issues are discussed in Sec. IV in the context of the one-band Hubbard model. In Sec. V,

we report results for this model that illustrate the accuracy and performance characteristics of our method. Finally, in Sec. VI, we summarize and discuss several simple extensions of the CPMC method.

II. BACKGROUND

In this section, we summarize the AFQMC method and also sketch a particular GFMC method, namely, the diffusion Monte Carlo (DMC) method,^{14,15} which is most analogous to our algorithm. In discussing the DMC method, the approach we use is not standard, but rather it is one designed to provide the necessary groundwork for the description of the CPMC method. Both the AFQMC and GFMC methods contain elements important to the CPMC method. For example, the basic techniques of the AFQMC method, such as Hubbard-Stratonovich transformation, imaginary-time propagation of Slater determinants, and matrix multiplication stabilization,^{9,11,17} are shared by the CPMC method; on the other hand, the random walk realization of the propagation,^{7,18} importance sampling in the random walks by use of a known trial function,^{3,7} and the fixed-node approximation¹⁴ are all GFMC concepts of much relevance.

Most ground-state quantum Monte Carlo methods are based on

$$|\psi_0\rangle \propto \lim_{\tau \rightarrow \infty} e^{-\tau H} |\psi_T\rangle; \quad (1)$$

that is, the ground state $|\psi_0\rangle$ can be projected from any known trial state $|\psi_T\rangle$ that satisfies $\langle \psi_T | \psi_0 \rangle \neq 0$. In a numerical method, the limit can be obtained iteratively by

$$|\psi^{(n+1)}\rangle = e^{-\Delta\tau H} |\psi^{(n)}\rangle, \quad (2)$$

where $|\psi^{(0)}\rangle = |\psi_T\rangle$. With a small $\Delta\tau$, the first-order Trotter approximation can be used:

$$e^{-\Delta\tau H} \approx e^{-\Delta\tau K} e^{-\Delta\tau V}. \quad (3)$$

Typically, K and V are the kinetic and potential energy operators. More generally, they are the one- and two-body interaction operators.

A. Auxiliary-field quantum Monte Carlo method

In the AFQMC method, the operators and wave function are in a second quantized representation, defined in terms of fermion creation and destruction operators c^\dagger and c . The basis is one of Slater determinants:

$$|\phi\rangle \equiv \phi_1^\dagger \phi_2^\dagger \cdots \phi_{N_\sigma}^\dagger |0\rangle, \quad (4)$$

where

$$\phi_i^\dagger \equiv \sum_j c_j^\dagger \Phi_{ji}. \quad (5)$$

Φ_{ji} are the elements of a matrix Φ of dimension $N \times N_\sigma$, where N is the size of the basis and N_σ is the number of fermions with spin σ . Each column of the matrix Φ represents a single-particle orbital that is completely specified by a vector of dimension N . One example of such a Slater determinant is the Hartree-Fock (HF) solution $|\phi_{\text{HF}}\rangle = \Pi_\sigma |\phi_{\text{HF}}^\sigma\rangle$, where each $|\phi_{\text{HF}}^\sigma\rangle$ is defined by a matrix

Φ_{HF}^σ whose columns are the N_σ lowest HF eigenstates. For any two real nonorthogonal Slater determinants $|\phi\rangle$ and $|\phi'\rangle$, it can be shown that their overlap integral

$$\langle \phi | \phi' \rangle = \det(\Phi^T \Phi') \quad (6)$$

and single-particle Green's function

$$G_{ij} \equiv \frac{\langle \phi | c_i c_j^\dagger | \phi' \rangle}{\langle \phi | \phi' \rangle} = \delta_{ij} - [\Phi' (\Phi^T \Phi')^{-1} \Phi^T]_{ij}. \quad (7)$$

Now we consider the projection (2) in this Slater-determinant basis. The trial wave function $|\psi_T\rangle$ can be a linear combination of determinants, but without loss of generality, we assume that it is a single determinant. A key point is that the projection of any Slater determinant by any operator of the form

$$\exp\left(\sum_{ij} c_i^\dagger M_{ij} c_j\right) \quad (8)$$

simply leads to another Slater determinant, i.e.,

$$\exp\left(\sum_{ij} c_i^\dagger M_{ij} c_j\right) |\phi\rangle = \phi'_1{}^\dagger \phi'_2{}^\dagger \cdots \phi'_{N_\sigma}{}^\dagger |0\rangle \equiv |\phi'\rangle, \quad (9)$$

with $\phi'_i{}^\dagger = \sum_j c_j^\dagger \Phi'_{ji}$ and $\Phi' \equiv e^{-M} \Phi$.

The $e^{-\Delta\tau K}$ part of Eq. (3) has this form. The $e^{-\Delta\tau V}$ part, however, does not as $V = 1/2 \sum_{ijkl} V_{ijkl} c_i^\dagger c_j^\dagger c_l c_k$. Following Hubbard, we rewrite V as a quadratic form:

$$V = \frac{1}{2} \sum_\alpha \lambda_\alpha \left(\sum_{ij} c_i^\dagger R_{ij}^\alpha c_j \right)^2 \equiv \frac{1}{2} \sum_\alpha \lambda_\alpha \rho_\alpha^2, \quad (10)$$

where the parameters λ_α and the matrix R^α are defined by the elements V_{ijkl} and the number of α is at most N^2 but is often much smaller. With this quadratic form, a Hubbard-Stratonovich (HS) transformation of the two-body part of Eq. (3) yields:

$$\begin{aligned} \exp\left(-\frac{1}{2} \Delta\tau \sum_\alpha \lambda_\alpha \rho_\alpha^2\right) &= \prod_\alpha \int_{-\infty}^{\infty} dx_\alpha \frac{e^{-x_\alpha^2/2}}{\sqrt{2\pi}} \\ &\times \exp\left(x_\alpha \sqrt{-\Delta\tau \lambda_\alpha} \sum_{ij} c_i^\dagger R_{ij}^\alpha c_j\right), \end{aligned} \quad (11)$$

where x_α is an auxiliary-field variable. Denoting the collection of such variables by \vec{x} and defining $B(\vec{x}) = \exp[-\Delta\tau \sum c_i^\dagger K_{ij} c_j] \prod_\alpha \exp[x_\alpha \sqrt{-\Delta\tau \lambda_\alpha} \sum c_i^\dagger R_{ij}^\alpha c_j]$, we obtain

$$e^{-\Delta\tau H} = \int d\vec{x} P(\vec{x}) B(\vec{x}), \quad (12)$$

where $P(\vec{x}) = \prod_\alpha (e^{-x_\alpha^2/2}/\sqrt{2\pi})$ is a probability density function and $B(\vec{x})$ has the desired form of Eq. (8). The essence of the HS transformation is the conversion of an interacting system into many *noninteracting* ones living in fluctuating external auxiliary fields, and the summation over all such auxiliary-field configurations recovers the correct many-body interactions. We note that different forms of this transforma-

tion exist¹⁹ and that they can affect the algorithm performance, possibly to a large degree. These issues are, however, not addressed here, as we will only be describing the general algorithm.

With Eqs. (2) and (12), the ground-state expectation $\langle \mathcal{O} \rangle$ of some observable \mathcal{O} can be computed by $\langle \psi^{(n)} | \mathcal{O} | \psi^{(n)} \rangle / \langle \psi^{(n)} | \psi^{(n)} \rangle$. The denominator is

$$\begin{aligned} & \langle \psi^{(0)} | e^{-n\Delta\tau H} e^{-n\Delta\tau H} | \psi^{(0)} \rangle \\ &= \int \langle \psi_T | \left[\prod_{l=1}^{2n} d\vec{x}^{(l)} P(\vec{x}^{(l)}) B(\vec{x}^{(l)}) \right] | \psi_T \rangle \quad (13) \\ &= \int \left[\prod_l d\vec{x}^{(l)} P(\vec{x}^{(l)}) \right] \det \left(\Psi_T^\top \prod_l \mathbf{B}(\vec{x}^{(l)}) \Psi_T \right), \quad (14) \end{aligned}$$

where $\mathbf{B}(\vec{x})$ is the $N \times N$ matrix associated with the single-particle operator $B(\vec{x})$ and Eqs. (6), (9), and (12) have been applied. In the AFQMC method,⁹ n is fixed and the many-dimensional integral in Eq. (14) is evaluated by a Monte Carlo (MC) method like the Metropolis algorithm. The MC process samples configurations $\{\vec{x}^{(1)}, \vec{x}^{(2)}, \dots, \vec{x}^{(2n)}\}$ of the auxiliary fields distributed according to the absolute value of the integrand.

In the AFQMC method, the sign problem occurs because in general the determinant in Eq. (14) is not always positive. In fact, its average sign approaches zero exponentially as n (or N) is increased.¹ The integral then becomes vanishingly small. Thus an *exponential* growth in computation time is required in its evaluation, since the MC samples, drawn from the *absolute value* of the integrand, become dominated by noise. This problem has remained largely uncontrolled, preventing general simulations at low temperatures or large system sizes.

One attempt to control the sign problem was the positive projection approximation proposed by Fahy and Hamann.¹³ They used a known wave function $|\psi_c\rangle$ and imposed $2n$ conditions

$$\langle \psi_T | B(\vec{x}^{(1)}) B(\vec{x}^{(2)}) \cdots B(\vec{x}^{(l)}) | \psi_c \rangle > 0, \quad l = 1, 2, \dots, n, \quad (15)$$

$$\begin{aligned} & \langle \psi_c | B(\vec{x}^{(l)}) B(\vec{x}^{(l+1)}) \cdots B(\vec{x}^{(2n)}) | \psi_T \rangle > 0, \\ & l = 2n, 2n-1, \dots, n+1, \quad (16) \end{aligned}$$

in sampling the auxiliary fields. The approximation is similar in spirit to that of the fixed-node approximation in the GFMC method. However, the constraint is *nonlocal* in imaginary time, as any change in $\vec{x}^{(l)}$ affects the constraint conditions at *all* times between l and n . Thus all auxiliary fields had to be updated simultaneously and only paths satisfying all constraining equations were accepted. The approach is hence computationally very intensive. In our CPMC method, we adopt the Fahy-Hamann concept of a constraining state but implement the constraint in the context of a random walk in the space of Slater determinants, which makes the procedure practical and straightforward.

B. Diffusion Monte Carlo method

The DMC method²⁰ executes the iteration in Eq. (2) as random walks in configuration space. When the fixed-point condition is reached, the random walks sample positions in configuration space from a distribution that represents the unknown *amplitude* of the ground-state wave function.

We denote the configuration basis by $|R\rangle$, where $R \equiv \{\vec{r}_1, \vec{r}_2, \dots, \vec{r}_{N_\sigma}\}$ is the electron coordinates in the continuous three-dimensional space. In this basis, the potential energy propagator $e^{-\Delta\tau V}$ in Eq. (3) is diagonal, but the kinetic energy propagator $e^{-\Delta\tau K}$, where $K = -\frac{1}{2} \sum_i \nabla_i^2$ is not. In order to write the latter in a more suitable form for a Monte Carlo treatment, we invoke a Hubbard-Stratonovich (HS) transformation:

$$e^{\Delta\tau \nabla_i^2 / 2} = \int dx_i \frac{e^{-x_i^2 / 2}}{(2\pi)^{1/2}} e^{\sqrt{\Delta\tau} x_i \cdot \nabla_i}. \quad (17)$$

Since $e^{\sqrt{\Delta\tau} x_i \cdot \nabla_i} |R\rangle$ displaces r_i in $|R\rangle$ by $\sqrt{\Delta\tau} x_i$, the effect of $e^{-\Delta\tau K}$ on any $|R\rangle$ can be viewed as ‘‘diffusing’’ it to $|R + \sqrt{\Delta\tau} \vec{x}\rangle$, where each component x_i of the auxiliary field \vec{x} is drawn from the normal distribution function $P(x_i) = e^{-x_i^2 / 2} / (2\pi)^{3/2}$.

The wave function $|\psi^{(n)}\rangle$ can be expressed in terms of the amplitudes $\langle R | \psi^{(n)} \rangle \equiv \psi^{(n)}(R)$. In the random walk realization of the iteration, $\psi^{(n)}(R)$ is represented by a finite ensemble of configurations $\{R_k^{(n)}\}$. At each stage, the Monte Carlo method provides the stochastic sampling of $\vec{x}_k^{(n)}$ and consequently the movement $|R_k^{(n)}\rangle \rightarrow |R_k^{(n)} + \sqrt{\Delta\tau} \vec{x}_k^{(n)}\rangle \equiv |R_k^{(n+1)}\rangle$ for each configuration in the ensemble. The factor $e^{-\Delta\tau V(R_k^{(n)})}$ translates into a weight (branching factor) for the configuration. As the iteration approaches the fixed-point condition, the weighted distribution of configurations represents $\psi_0(R) = \langle R | \psi_0 \rangle$.

The sign problem in the DMC method has a somewhat different character than the sign problem in the AFQMC method. The Pauli exclusion principle requires that the fermion wave function $\psi_0(R)$ change sign if the positions of two electrons with the same spin are interchanged. Unlike the AFQMC method, the straightforward DMC method does not impose the antisymmetric property in the projection process. Without additional mechanisms, the DMC method naturally produces points distributed according to the lowest eigenstate of the diffusion equation. This state is symmetric and bosoniclike. There has only been limited success in attempts to construct exact algorithms that yield asymptotically (in n) a nonvanishing, antisymmetric Monte Carlo signal.^{21,22}

The fixed-node method^{14–16} is an approximate scheme to prevent the convergence to the bosoniclike ground state. Antisymmetry in $\psi_0(R)$ implies that there are equivalent regions in configuration space which are separated by a nodal surface on which $\psi_0(R) = 0$. The exact nodal surface is in general unknown. In the fixed-node approximation, a trial nodal surface is assumed, based on a known trial wave function $|\psi_T\rangle$. A solution which is everywhere positive is then sought in the region $\psi_T(R) > 0$ by imposing the boundary condition that $\psi^{(n)}(R)$ vanish at $\psi_T(R) = 0$. Unless $\psi_T(R) = 0$ happens to be the correct node, the resulting DMC

solution for the ground state is approximate. The ground-state energy obtained is an upper bound.¹⁵

An important feature of the DMC method is importance sampling. This technique is necessary to reduce the variance of the computed results to acceptable levels. For brevity we will not discuss this technique here. Instead, we will postpone such a discussion until it is needed to complete our description of the CPMC algorithm.

III. CONSTRAINED PATH MONTE CARLO METHOD

We now describe the CPMC algorithm. It uses the Hubbard-Stratonovich-based formalism of the AFQMC method, but a Monte Carlo sampling procedure similar to that of the DMC method. The iterative process (2) becomes an open-ended random walk in *Slater-determinant space*. Within the framework of this random walk, we introduce importance sampling and the constrained path approximation.

We remark that any antisymmetric wave function can be written as a linear combination of Slater determinants, i.e.,

$$|\psi\rangle = \sum_{\phi} \chi_{\psi}(\phi) |\phi\rangle, \quad (18)$$

where the sum is over each member of the Slater determinant basis. As introduced in Sec. II, we will always use $|\psi\rangle$ to denote antisymmetric wave functions and $|\phi\rangle$ to denote a single Slater determinant. Contrary to the configuration space used in the DMC method, the Slater-determinant basis space of $|\phi\rangle$ is *nonorthogonal* and *overcomplete*.

A. Importance-sampled random walk formulation

Using Eq. (12), we write the iterative equation (2) as

$$|\psi^{(n+1)}\rangle = \int d\vec{x} P(\vec{x}) B(\vec{x}) |\psi^{(n)}\rangle. \quad (19)$$

In the Monte Carlo realization of this iteration, we represent the wave function at each stage by a finite ensemble of Slater determinants, i.e.,

$$|\psi^{(n)}\rangle \propto \sum_k |\phi_k^{(n)}\rangle. \quad (20)$$

Here k labels the Slater determinants and an overall normalization factor of the wave function has been omitted. The Slater determinants are referred to as *random walkers* as they are generated by the random walk. At any stage of the iteration, the sum will be over only part of the basis as the determinants in this sum are statistical samples whose distribution represents the linear coefficient $\chi_{\psi^{(n)}}$ in Eq. (18). The statistical accuracy of this representation increases algebraically as the number of independent samples is increased. In the remainder of the paper, Eq. (20) will serve as the definition of the Monte Carlo representation of a wave function in the CPMC method. We will start from an initial ensemble where, for each k , $|\phi_k^{(0)}\rangle = |\psi_T\rangle$.²³

One step of the iteration involves the propagation of each walker according to Eq. (19). Since the noninteracting operator $B(\vec{x})$ operating on any Slater determinant leads to another Slater determinant, an analytical realization of this propaga-

tion for each walker would yield a linear combination of many Slater determinants. In our random walk, this propagation is achieved stochastically by Monte Carlo sampling of \vec{x} :

$$|\phi_k^{(n+1)}\rangle \leftarrow \int d\vec{x} P(\vec{x}) B(\vec{x}) |\phi_k^{(n)}\rangle; \quad (21)$$

that is, for each random walker we choose an auxiliary-field configuration \vec{x} from the probability density function $P(\vec{x})$ and propagate the walker to a new one via $|\phi_k^{(n+1)}\rangle = B(\vec{x}) |\phi_k^{(n)}\rangle$. We repeat this procedure for *all* walkers in the population. These operations accomplish one step of the random walk. The new population represents $|\psi^{(n+1)}\rangle$ in the sense of Eq. (20), i.e., $|\psi^{(n+1)}\rangle \propto \sum_k |\phi_k^{(n+1)}\rangle$. These steps are iterated indefinitely. After an equilibration phase, all walkers thereon are MC samples of the ground-state wave function $|\psi_0\rangle$ and ground-state properties can be computed.

In order to improve the efficiency of Eq. (19) and make it a practical algorithm, an importance sampling scheme is required. In the procedure just described, no information is contained in the sampling of \vec{x} on the importance of the resulting determinant in representing $|\psi_0\rangle$, yet such information is clearly important. For example, the ground-state energy is given by $E_0 \equiv \langle \psi_T | H | \psi_0 \rangle / \langle \psi_T | \psi_0 \rangle$. Hence, estimating E_0 requires estimating the denominator by $\sum_{\phi} \langle \psi_T | \phi \rangle$, in which $|\phi\rangle$ denotes random walkers after equilibration. Since these walkers are sampled with no knowledge of $\langle \psi_T | \phi \rangle$, terms in the summation over ϕ can have large fluctuations that lead to large statistical errors in the MC estimate of the denominator, thereby in that of E_0 .

To introduce importance sampling, we iterate a modified equation with a modified wave function, without changing the underlying eigenvalue problem of Eq. (19). Specifically, for each Slater determinant $|\phi\rangle$, we define an importance function

$$O_T(\phi) \equiv \langle \psi_T | \phi \rangle, \quad (22)$$

which estimates its overlap with the ground-state wave function. We can then rewrite Eq. (19) as

$$|\tilde{\psi}^{(n+1)}\rangle = \int d\vec{x} \tilde{P}(\vec{x}) B(\vec{x}) |\tilde{\psi}^{(n)}\rangle, \quad (23)$$

where the modified wave function is

$$|\tilde{\psi}^{(n)}\rangle = \sum_{\phi} O_T(\phi) \chi_{\psi^{(n)}}(\phi) |\phi\rangle \quad (24)$$

and the modified ‘‘probability density function’’ is

$$\tilde{P}(\vec{x}) = \frac{O_T(\phi^{(n+1)})}{O_T(\phi^{(n)})} P(\vec{x}). \quad (25)$$

We note that $\tilde{P}(\vec{x})$ is a function of both the future $|\phi^{(n+1)}\rangle$ and the current $|\phi^{(n)}\rangle$ positions in Slater-determinant space. It is trivially verified that Eqs. (19) and (23) are identical.

In the random walk, the ensemble of walkers $\{|\phi_k^{(n)}\rangle\}$ now represents the modified wave function $|\tilde{\psi}^{(n)}\rangle \propto \sum_k |\phi_k^{(n)}\rangle$, which is to say that their distribution represents

the function $O_{T\chi\psi^{(n)}}$. The iterative relation for each walker is again given by Eq. (21), but with $P(\vec{x})$ replaced by $\tilde{P}(\vec{x})$. The latter is in general not a normalized probability density function, and we denote the normalization constant for walker k by $N(\phi_k^{(n)})$ and rewrite Eq. (21) as

$$|\phi_k^{(n+1)}\rangle \leftarrow N(\phi_k^{(n)}) \int d\vec{x} \frac{\tilde{P}(\vec{x})}{N(\phi_k^{(n)})} B(\vec{x}) |\phi_k^{(n)}\rangle. \quad (26)$$

This iteration now forms the basis of the CPMC algorithm. As in the DMC method, it is convenient to associate a weight $w_k^{(n)}$ with each walker, which can be initialized to unity. One step of the random walk is then as follows: For each walker $|\phi_k^{(n)}\rangle$, (i) sample a \vec{x} from the probability density function $\tilde{P}(\vec{x})/N(\phi_k^{(n)})$, (ii) propagate the walker by $B(\vec{x})$ to generate a new walker, and (iii) compute a weight $w_k^{(n+1)} = w_k^{(n)} N(\phi_k^{(n)})$ for the new walker. With the introduction of the weight, $|\tilde{\psi}^{(n)}\rangle \propto \sum_k w_k^{(n)} |\phi_k^{(n)}\rangle$.

Steps (i) and (iii) are sometimes difficult to implement. To ease their implementation, we apply the HS transformation of Eqs. (23) and (25) to *each* component of \vec{x} . This application is simple since both $P(\vec{x})$ and $B(\vec{x})$ can be decomposed into a product of independent factors corresponding to individual components x_α . Every step of the random walk then consists of successive substeps in which the x_α are sampled one by one, each according to (i)–(iii). As we discuss in Sec. IV, such a decomposition is adequate to make the Hubbard-model application straightforward, since the HS transformation we use allows only two discrete values (± 1) for each x_α and, thus, the easy tabulation of $\tilde{P}(x_\alpha)$. For more general cases, however, it is often necessary to further approximate $\tilde{P}(x_\alpha)$. The following procedure can be adopted: Under the assumption of small $\Delta\tau$, the ratio of the overlap integrals is manipulated into the form of an exponential whose exponent is linear in x_α ; $\tilde{P}(x_\alpha)$ is then written as a shifted Gaussian times a normalization constant. The basic idea of this procedure is similar to that used in the DMC method.

To better see the effect of importance sampling, we observe that if $|\psi_T\rangle = |\psi_0\rangle$, the normalization $\int \tilde{P}(\vec{x}) d\vec{x}$ is constant. Therefore the weights of walkers remain a constant and the random walk has no fluctuation. Furthermore, we refer again to the estimator for E_0 . With importance sampling, the denominator becomes the sum of weights w , while the numerator is $\sum_\phi \langle \psi_T | H | \phi \rangle w_\phi / \langle \psi_T | \phi \rangle$, where again $|\phi\rangle$ denotes walkers after equilibration. As $|\psi_T\rangle$ approaches $|\psi_0\rangle$, all walkers contribute equally to the estimator and the variance approaches zero. We emphasize that different choices of importance functions only affect the efficiency of the calculation.

B. Constrained path approximation

Despite the advantages over the standard AFQMC method in terms of sampling efficiency, the random walk formulation still suffers from the sign problem. Here we will illustrate the origin of the sign problem in this framework and then introduce the constrained path approximation to eliminate the exponential decay of the average sign. We will see that while a fixed-node-like approximation has proved

difficult to implement effectively in standard AFQMC method,¹³ it is extremely simple to implement under our random walk formulation.

The sign problem occurs because of the fundamental symmetry existing between the fermion ground state $|\psi_0\rangle$ and its negative $-|\psi_0\rangle$.^{13,21} For any ensemble of Slater determinants $\{|\phi\rangle\}$ which gives a Monte Carlo representation of the ground-state wave function, this symmetry implies that there exists another ensemble $\{-|\phi\rangle\}$ which is also a correct representation. In other words, the Slater-determinant space can be divided into two degenerate halves (+ and -) whose bounding surface \mathcal{N} is defined by $\langle \psi_0 | \phi \rangle = 0$ and is in general *unknown*.

In some special cases, such as the particle-hole symmetric, half-filled one-band Hubbard model, symmetry prohibits any crossing of \mathcal{N} in the random walk. The calculation is then free of the sign problem.²⁵ In more general cases, walkers *can* cross \mathcal{N} in their propagation by $e^{-\Delta\tau H}$. The sign problem then invariably occurs. Once a random walker reaches \mathcal{N} , it will make no further contribution to the representation of the ground state since

$$\langle \psi_0 | \phi \rangle = 0 \Rightarrow \langle \psi_0 | e^{-\tau H} | \phi \rangle = 0 \quad \text{for any } \tau. \quad (27)$$

Paths that result from such a walker have equal probability of being in either half of the Slater-determinant space. Computed analytically, they would cancel, but without any knowledge of \mathcal{N} , they continue to be sampled in the random walk and become Monte Carlo noise. At sufficiently large n , the Monte Carlo representation of the ground-state wave function consists of an *equal* mixture of the + and - ensembles, regardless of where the random walks originated. The Monte Carlo signal is therefore lost. The decay of the signal-to-noise ratio, i.e., the decay of the average sign of $\langle \psi_T | \phi \rangle$, occurs at an exponential rate with imaginary time.

In this regard, the fermion sign problem appears very similar in either the DMC, AFQMC, or CPMC algorithms. The difference between the algorithms is that in the DMC algorithm minus signs appear when particles interchange positions in configuration space while in the CPMC and AFQMC algorithms the orbitals must interchange. The orbitals are an extended quantity and hence, at least for systems near a mean-field solution, the fermion sign problem is reduced.

To eliminate the decay of the signal-to-noise ratio, we impose the constrained path approximation. It requires that each random walker at each step have a positive overlap with the trial wave function $|\psi_T\rangle$:

$$\langle \psi_T | \phi_k^{(n)} \rangle > 0. \quad (28)$$

This yields an approximate solution to the ground-state wave function, $|\psi_0^c\rangle = \sum_\phi |\phi\rangle$, in which all Slater determinants $|\phi\rangle$ satisfy Eq. (28). From Eq. (27), it follows that this approximation becomes *exact* for an exact trial wave function $|\psi_T\rangle = |\psi_0\rangle$.²⁶

As a consequence of the constrained path approximation, the ground-state energy E_0^c , computed by the estimator discussed in Sec. III A, is an upper bound to the true value E_0 . To see this, we introduce an antisymmetrization operator A_ϕ in the Slater-determinant space that extends any wave function defined in half the space by $\sum_\phi |\phi\rangle$ into the whole

space by $\Sigma_{\phi}|\phi\rangle - \Sigma_{-\phi}|\phi\rangle$. Since $A_{\phi}|\psi_0^c\rangle$ is an eigenfunction of the modified Hamiltonian $H^c = H + V^c$, where V^c is ∞ at \mathcal{N} and 0 elsewhere, we have $H^c(A_{\phi}|\psi_0^c\rangle) = H(A_{\phi}|\psi_0^c\rangle) = E_0'(A_{\phi}|\psi_0^c\rangle)$. Both $A_{\phi}|\psi_0^c\rangle$ and $A_{\phi}|\psi_0\rangle$ reside in the same Slater-determinant space and both are anti-symmetric functions. Thus $E_0^c \geq E_0$. On the other hand, we recall that

$$E_0^c \equiv \frac{\langle \psi_T | H | \psi_0^c \rangle}{\langle \psi_T | \psi_0^c \rangle} = \frac{\langle \psi_T | H A_{\phi} | \psi_0^c \rangle}{\langle \psi_T | A_{\phi} | \psi_0^c \rangle}. \quad (29)$$

Therefore $E_0^c = E_0'$ and $E_0^c \geq E_0$.

To implement the constrained path approximation in the random walk, we redefine the importance function by Eq. (22):

$$O_T(\phi) \equiv \max\{\langle \psi_T | \phi \rangle, 0\}. \quad (30)$$

This prevents walkers from crossing the trial nodal surface \mathcal{N} and entering the “-” half-space as defined by $|\psi_T\rangle$. In the limit $\Delta\tau \rightarrow 0$, Eq. (30) ensures that the walker distribution vanishes smoothly at \mathcal{N} and the constrained path approximation is properly imposed. With a finite $\Delta\tau$, however, $\tilde{P}(\vec{x})$ has a discontinuity at \mathcal{N} and the distribution does not vanish. We have found this effect to be very small for reasonably small imaginary-time steps $\Delta\tau$. Nonetheless, we correct for it by modifying $\tilde{P}(\vec{x})$ near \mathcal{N} so that it approaches zero smoothly at \mathcal{N} . As we discuss in Sec. IV, the procedure is analogous to the mirror correction^{16,20} used in the DMC method.

C. Computing expectation values

After the random walk has equilibrated, the distribution of random walkers represents the ground-state wave function $|\psi_0^c\rangle$ under the constrained path approximation. Various expectation values can then be computed from a population of these walkers and their weights. For example, the ground-state energy is

$$\begin{aligned} E_0^c &= \frac{\langle \psi_T | H | \psi_0^c \rangle}{\langle \psi_T | \psi_0^c \rangle} = \frac{\sum_{\phi} O_T(\phi) \chi(\phi) \langle \psi_T | H | \phi \rangle / O_T(\phi)}{\sum_{\phi} O_T(\phi) \chi(\phi) \langle \psi_T | \phi \rangle / O_T(\phi)} \\ &\simeq \frac{\sum_k w_k \langle \psi_T | H | \phi_k \rangle / \langle \psi_T | \phi_k \rangle}{\sum_k w_k}, \end{aligned} \quad (31)$$

where terms in the numerator $\langle \psi_T | H | \phi_k \rangle / \langle \psi_T | \phi_k \rangle$ are given by combinations of elements of the Green’s function as defined in Eq. (7).

An estimator similar to Eq. (31), namely, $\langle \psi_T | \mathcal{O} | \psi_0^c \rangle / \langle \psi_T | \psi_0^c \rangle$, is easily obtained for any other operator \mathcal{O} . In the GFMC method, this type of estimator is referred to as the *mixed* estimator. We recall that the true expectation value of \mathcal{O} with respect to $|\psi_0^c\rangle$ is

$$\langle \mathcal{O} \rangle^c = \frac{\langle \psi_0^c | \mathcal{O} | \psi_0^c \rangle}{\langle \psi_0^c | \psi_0^c \rangle}. \quad (32)$$

For the energy, the mixed estimator is equivalent to the true estimator (32), but this is not true for any \mathcal{O} that does not commute with H . In this case, it is sometimes possible to improve the mixed estimator by the linear extrapolation³

$$\langle \mathcal{O} \rangle_{\text{extrap}} \approx 2\langle \mathcal{O} \rangle_{\text{mixed}} - \langle \mathcal{O} \rangle_{\text{var}}, \quad (33)$$

where the variational estimate $\langle \mathcal{O} \rangle_{\text{var}} = \langle \psi_T | \mathcal{O} | \psi_T \rangle / \langle \psi_T | \psi_T \rangle$.

Even a good trial wave function $|\psi_T\rangle$ with a good variational energy can sometimes fail to give a reasonable estimate for certain correlation functions. In such cases, Eq. (33) will not be effective. It is then imperative to compute Eq. (32). To do this, we devised a scheme called *back propagation* (BP), the essence of which comes from the forward-walking (FW) technique¹⁸ in the GFMC method:

$$\langle \mathcal{O} \rangle_{\text{BP}} = \lim_{\tau \rightarrow \infty} \frac{\langle \psi_T \exp(-\tau H_c) | \mathcal{O} | \psi_0^c \rangle}{\langle \psi_T \exp(-\tau H_c) | \psi_0^c \rangle}. \quad (34)$$

A subtle distinction, however, exists between back propagation and forward walking. In back propagation, $\langle \psi_T \exp(-\tau H_c) | = \langle \psi_T | \exp(-\tau H_c)$ is restricted to “constrained” paths, i.e., those paths that do not violate the constraint in the *original forward direction* $\exp(-\Delta\tau H_c) | \psi_0^c \rangle$. In the DMC method a path in configuration space has no sense of direction with respect to the nodal surface. In the CPMC method, however, there is a sense of direction: A set of determinants along the path of a random walk which does not violate the constraint at any step when going from right to left may indeed violate it any even number of times when going from left to right.

Because of this sense of direction, expression (34) may not yield Eq. (32). However, since $|\psi_0^c\rangle$ is itself approximate, this issue is not crucial. What is crucial is that $\langle \mathcal{O} \rangle_{\text{BP}}$ remains exact for an exact trial wave function. To demonstrate that it does, we will use perturbation theory and start by considering a Hamiltonian

$$H' = H + \lambda \mathcal{O}, \quad (35)$$

where \mathcal{O} is the operator whose expectation value we seek. We then apply the CPMC method to the new Hamiltonian H' with a new constraint governed by $|\psi_T'\rangle$, where

$$|\psi_T'\rangle = |\psi_T\rangle + \lambda |\delta\psi_T\rangle, \quad (36)$$

and $|\delta\psi_T\rangle$ is orthogonal to $|\psi_T\rangle$, i.e., $\langle \psi_T' | \psi_T \rangle = \langle \psi_T | \psi_T \rangle$, which is the standard boundary condition of perturbation theory. In the limit of small λ , the constraint becomes identical to that of the original Hamiltonian H . To first order in λ , we thus simply regain the previous expression (34) for $\langle \mathcal{O} \rangle_{\text{BP}}$. The term proportional to $|\delta\psi_T\rangle$ does not contribute because it is orthogonal to the true ground state.

Numerically we compared $\langle \mathcal{O} \rangle_{\text{BP}}$ with $\langle \mathcal{O} \rangle^c$ in several simple cases and observed reasonable agreement. In principle we can compute $\langle \mathcal{O} \rangle^c$ by creating a separate walk for the left-hand wave function, which propagates from $\langle \psi_T |$ with an appropriate sense of direction, and then matching it with populations in the regular (right-hand) walk. In practice, however, it is difficult for such a scheme to yield accurate results, due to a lack of proper importance sampling.²⁷

Neither of the above measurement procedures is free from bias in the long imaginary-time limit. Since we are dealing with a branching random walk, there is necessarily a bias that arises from finite population sizes. However, this bias can be greatly reduced by taking a relatively large population size (a few hundred to a few thousand). The convergence and

amount of bias will depend upon $|\psi_T\rangle$ and the low-energy excitations of the system. We have found the back-propagation estimate of ground-state observables to be both statistically and physically accurate in our Hubbard model calculations.

It is relatively simple to implement the back-propagation scheme on top of a regular CPMC calculation. We choose an iteration n and store the entire population $\{|\phi_k^{(n)}\rangle\}$. As the random walk proceeds, we keep track of the following two items for each new walker: (1) the sampled auxiliary-field variables that led to the new walker from its parent walker and (2) an integer that labels the parent. After an additional m iterations, we carry out the back propagation: For each walker l in the $(n+m)$ th (current) population, we initiate a determinant $\langle\psi_T|$ and act on it with the corresponding propagators, but taken in reverse order. The m successive propagators are constructed from the stored items, with $\exp(-\Delta\tau K/2)$ inserted where necessary. The resulting determinants $\langle\bar{\phi}_l^{(m)}|$ are combined with its parent from iteration n to compute $\langle\mathcal{O}\rangle_{\text{BP}}$, in a way similar to the mixed estimator (31). The weights are given correctly by $w_l^{(n+m)}$ due to importance sampling in the regular walk. Starting from another iteration n' , this process can be repeated and the results accumulated.

IV. IMPLEMENTATION ISSUES: THE HUBBARD MODEL

The one-band Hubbard model is a simple paradigm of a system of interacting electrons. Its Hamiltonian is given by

$$H = K + V = -t \sum_{\langle ij \rangle \sigma} (c_{i\sigma}^\dagger c_{j\sigma} + c_{j\sigma}^\dagger c_{i\sigma}) + U \sum_i n_{i\uparrow} n_{i\downarrow}, \quad (37)$$

where t is the overlap integral, $U > 0$ is the on-site Coulomb repulsion, $n_{i\sigma} = c_{i\sigma}^\dagger c_{i\sigma}$, and the angular brackets indicate near neighbors. We will take $t=1$ and assume a two-dimensional square lattice of size $N=L \times L$, with periodic boundary conditions.

The physics of this model is rich, containing magnetism, a metal-insulator transition, and heavy Fermion behavior. Originally the model was proposed for ferromagnetism; today's interest focuses on the extent to which it might exhibit superconductivity away from the half-filled case of $N_\uparrow = N_\downarrow = N/2$. It is in the electron- and hole-doped regions around half-filling that existing QMC methods experience a debilitating sign problem that restricts the simulations to small lattice sizes. In another paper, we will detail our study of the physical properties of this model.²⁴

To illustrate the CPMC algorithm in more detail, we now describe our implementation of it for the Hubbard Hamiltonian. For this and related lattice models, we use the discrete version²⁵ of the Hubbard-Stratonovich transformation

$$e^{-\Delta\tau U n_{i\uparrow} n_{i\downarrow}} = e^{-\Delta\tau U (n_{i\uparrow} + n_{i\downarrow})/2} \sum_{x_i = \pm 1} p(x_i) e^{\gamma x_i (n_{i\uparrow} - n_{i\downarrow})}, \quad (38)$$

where $\cosh(\gamma) = \exp(\Delta\tau U/2)$ and the probability density function $p(x_i) = 1/2$ allows only $x_i = \pm 1$. Here we label

components of the auxiliary field \vec{x} by i , instead of by α , because of their one-to-one correspondence with lattice sites.

A. Specific issues

Each Slater determinant $|\phi\rangle = |\phi^\uparrow\rangle|\phi^\downarrow\rangle$, and similarly $B(\vec{x}) = B^\uparrow(\vec{x})B^\downarrow(\vec{x})$. Any overlap integral between two Slater determinants involves the product of overlaps of individual spin determinants, e.g., $\langle\psi_T|\phi\rangle = \prod_\sigma \langle\psi_T^\sigma|\phi^\sigma\rangle$. Reflective of the interaction, the \uparrow and \downarrow spin determinants share auxiliary fields. Aside from this connection, they propagate independently. With these details about electron spin taken into consideration, all our previous discussions directly apply.

To reduce errors associated with the first-order Trotter approximation (3), we use the second-order symmetric form $\exp(-\Delta\tau H) \approx \exp(-\Delta\tau K/2) \exp(-\Delta\tau V) \exp(-\Delta\tau K/2)$. Thus,

$$B(\vec{x}) = B_{K/2} B_V(\vec{x}) B_{K/2}, \quad (39)$$

where $B_V(\vec{x})$ is the auxiliary-field-dependent propagator from the HS transformation. From Eq. (38), $B_V^\sigma(\vec{x}) = \prod_i b_V^\sigma(x_i)$, where

$$b_V^\sigma(x_i) = e^{-[\Delta\tau U/2 + s(\sigma)\gamma x_i] c_{i\sigma}^\dagger c_{i\sigma}}, \quad (40)$$

with $s(\uparrow) = 1$ and $s(\downarrow) = -1$, and $B_{K/2}^\sigma = e^{-\Delta\tau K\sigma/2}$. The probability density function is $P(\vec{x}) = \prod_i p(x_i)$.

For a walker $|\phi\rangle$, we now describe one substep of the random walk in which the i th component x_i of the HS field is sampled and then $b_V(x_i)$ is applied to the walker. If $b_V(x_i)|\phi\rangle$ is denoted by $|\phi'\rangle$, we have

$$\bar{p}(x_i) = \frac{O_T(\phi')}{O_T(\phi)} p(x_i). \quad (41)$$

Thus the probability of picking one of the two possible values of x_i is $\bar{p}(x_i)/[\bar{p}(+1) + \bar{p}(-1)]$. Once an x_i is chosen, $|\phi\rangle$ is propagated to obtain a new walker and the new weight is $w[\bar{p}(+1) + \bar{p}(-1)]$. Since $\mathbf{b}_V^\sigma(x_i)$ modifies only one row of the matrix Φ^σ , it is straightforward and inexpensive to compute the resulting ratio of determinants for each of the two possible values of x_i , provided the inverse of the overlap matrix $(\Psi_T^T \Phi^\sigma)^{-1}$ is known. As one moves to the next i , the overlap matrix can be efficiently updated by procedures that are almost identical to ones used in the AFQMC method.^{9,11}

As we mentioned in Sec. III B, with a finite $\Delta\tau$, Eq. (30) causes $\bar{p}(x_i)$ to be discontinuous at \mathcal{N} . To correct for this, we include a simple ‘‘mirror-correction’’ procedure in the above substep: If walker $|\phi\rangle$ is close to \mathcal{N} , where we define ‘‘close’’ as when one application of $b_V(x_i)$ (with either x_i) would lead to a determinant $|\phi'\rangle$ with a negative overlap with $|\psi_T\rangle$, we modify its weight to $w/[1 - \langle\psi_T|\phi'\rangle/O_T(\phi)]$. After the new walker $|\phi'\rangle$ has been accepted, we again check whether it is close to \mathcal{N} . This is done by applying $b_V(x_i)$ one additional time with the chosen x_i . Similar to w above, the weight w' is modified to $w'/[1 - \langle\psi_T|b_V(x_i)|\phi'\rangle/\langle\psi_T|\phi'\rangle]$ if the overlap $\langle\psi_T|b_V(x_i)|\phi'\rangle$ is negative. We note that there is essentially no computational cost in computing this overlap.

B. Algorithm outline

The basic steps of the algorithm are the following.

(1) For each walker, specify its initial state to be some appropriate Ψ_T and assign its weight w and overlap O_T each a value of unity.

(2) If the weight of the walker is nonzero, propagate it via

$B_{K/2}$.

(a) Perform the matrix-matrix multiplication

$$\Phi' = \mathbf{B}_{K/2} \Phi \quad (42)$$

and compute the new importance function

$$O'_T = O_T(\phi'). \quad (43)$$

(b) If $O'_T \neq 0$, update the walker, weight, and O_T :

$$\Phi \leftarrow \Phi', \quad w \leftarrow w O'_T / O_T, \quad O_T \leftarrow O'_T. \quad (44)$$

(3) If the walker's weight is still nonzero, propagate it via $B_V(\vec{x}) = \prod_j b_V(x_j)$.

(a) Compute the inverse of the overlap matrix

$$\mathbf{O}_{\text{inv}} = (\Psi_T^T \Phi)^{-1}. \quad (45)$$

(b) For *each* auxiliary field x_i ($i=1, N$) do the following.

(i) Compute $\tilde{p}(x_i)$ in which the ratio with O_T can be expressed in terms of x_i and the Green's function element G_{ii} as defined in Eq. (7).

(ii) Sample x_i and update the weight according to the discussion in Sec. IV A.

(iii) If the weight of the walker is still not zero, propagate the walker by $\mathbf{b}_V(x_i)$ and then update O_T and \mathbf{O}_{inv} .

(iv) Apply the mirror correction in step (i) or (iii) if necessary.

(4) Repeat step (2).

(5) Include an overall normalization factor in walker weight: $w \leftarrow w e^{\Delta \tau E_T}$, where E_T is an estimate of E_0 .

(6) Repeat steps (2)–(5), which form one step of the random walk, for all walkers in the population.

(7) If the population of walkers has achieved a steady-state distribution, periodically make estimates of physical quantities.

(8) Periodically adjust the population of walkers.

(9) Periodically reorthonormalize the columns of all the Φ with nonzero weights.

(10) Cycle the process until an adequate number of measurements are collected.

(11) Compute final averages, estimate their statistical error, and stop.

We omitted the spin index σ , but identical operations for both electron spin determinants are implied whenever a matrix manipulation is described. In presenting the above steps, we focused on illustrating the algorithm; the outline does not represent the most efficient implementation.

We also ignored back propagation. To implement it, an additional procedure is required in each random walk step in the measurement phase. As discussed at the end of Sec. III C, this procedure takes *one* of the following three possibilities:

(i) storing all walkers [step (6)], (ii) storing ancestry links [step (3)], and auxiliary fields [step (3 b iii)] for each walker, and copying them if necessary [step (8)], or (iii) back propa-

gating from $\langle \psi_T |$, computing $\langle \mathcal{O} \rangle_{\text{BP}}$, and accumulating results [step (6)]. The length m of the back propagation is preset as are the number of iterations in each measurement block, the frequency of measurements, etc.

Additionally, we introduced several previously undiscussed steps and procedures. We now discuss these.

C. Additional algorithmic issues

In this section, we discuss the use of E_T , the growth estimator, population control, and reorthogonalization. Variants of the first three are present in all GFMC calculations, while the last one is adopted from the AFQMC method. We merely highlight these issues in the context of algorithm and point to references with more extensive discussions. While we will refer to the outline for the Hubbard implementation in Sec. IV B, the issues are general.

As shown in step (5), a constant $e^{\Delta \tau E_T}$ multiplies the propagator $e^{-\Delta \tau H}$. If $E_T = E_0^c$, the steady-state eigenvalue of Eq. (2) is unity. In other words, after equilibration the total weight of walkers remains a constant on the average. An inaccurate input of E_T is only a minor concern, since the value of E_T simply changes the total weight systematically by a constant factor. A statistical estimate of this factor is easily obtained from the random walk by observing the total weights through a number of iterations.³ On the average these totals scale as $\exp[-\Delta \tau (E_0^c - E_T)]$ and hence provide an estimate of E_0^c . This procedure for estimating the ground-state energy is often referred to as the *growth estimator*.

In the random walk, one walker will eventually dominate all others and the random walk will spend most of its time sampling walkers which contribute little. To avoid such a loss of efficiency, a population control procedure²⁰ is needed [step (8)]. First, a branching (or birth and death) scheme is applied, in which walkers with large weights are replicated and ones with small weights are eliminated with some probability. There exist various ways to do this,^{3,20,28} with the guideline being that the process should not affect the distribution statistically. Branching allows the total number of walkers to fluctuate and possibly become too large or too small. Thus, as a second step, the population size is adjusted, if necessary, by rescaling the weights with an overall factor. Readjusting the population size introduces a bias and should only be done infrequently. If this is not possible due to a poor $|\psi_T\rangle$ or poor importance sampling, several calculations must be done with different (average) population sizes in order to extrapolate to the infinite population limit.

The overall structure of that of a CPMC calculation resembles a typical GFMC calculation.³ After equilibration, we introduce an intermediate phase in which the growth estimator is computed. The length of this phase is a parameter and the outcome is used to adjust E_T . The new value of E_T is then used in the next phase, which is divided into independent blocks. Because of the correlated nature of successive steps, measurements are made only at suitable intervals. At an iteration n when measurements are taken, the average of a quantity \mathcal{O} is $\mathcal{O}^{(n)} = u^{(n)} / d^{(n)}$. In each block, we do not accumulate $\mathcal{O}^{(n)}$. Instead we accumulate $u^{(n)}$ and $d^{(n)}$ separately and compute a final average at the end of the block. The final result and statistical error estimate [step (11)] are obtained from these bin averages.

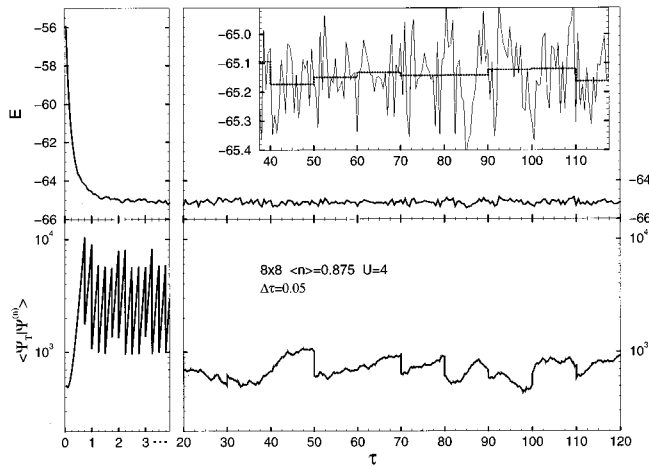


FIG. 1. Stability and convergence of the CPMC method. In the lower half of the figure is the overlap integral $\langle \psi_T | \psi^{(n)} \rangle$ as a function of the imaginary time $\tau = n \Delta \tau$, where n labels the random walk step. In the presence of the sign problem, this overlap integral would decay exponentially with n . In the upper half of the figure is the corresponding estimate of the total energy as a function of n . The inset is an enlarged version of the portion between $\tau = 37.5$ and $\tau = 117.5$ in which the dotted line indicates the computed energy value from blocks of length $\tau = 10$. This calculation yielded a ground-state energy of $E_0^c = -65.135 \pm 0.008$, compared to an AFQMC result (Ref. 29) of -65.02 ± 0.06 .

Step (9) is prompted by the fact that the repeated multiplication of $\mathbf{B}(\vec{x})$ leads to a numerical instability: A relatively quickly numerical error grows to the point where $|\phi_k^{(n)}\rangle$ represents an unfaithful propagation of $|\phi_k^{(0)}\rangle$. This instability is well known in the AFQMC method and is controlled^{11,17} by a numerical stabilization technique that requires the periodic reorthonormalization of the single-particle orbitals in $|\phi_k^{(n)}\rangle$. In our calculation, we use the *modified* Gram-Schmidt procedure^{11,17} which for each walker $|\phi\rangle$ factors the matrix Φ as $\Phi = \mathbf{Q}\mathbf{R}$, where \mathbf{Q} is a matrix whose columns are a set of orthonormal vectors and \mathbf{R} is a triangular matrix. After this factorization, Φ is replaced by \mathbf{Q} and the corresponding overlap O_T is replaced by $O_T / \det(\mathbf{R})$.

V. RESULTS

We have presented a rather detailed discussion of the constrained path Monte Carlo method to make the CPMC algorithm as transparent as possible. In this section we present a variety of results from simulations of the Hubbard model that are chosen primarily for their importance in illustrating algorithmic issues. These results are for two-chain and two-dimensional lattices. First, we give results for the ground-state energy as a function of system size N , filling fraction $\langle n \rangle = (N_\uparrow + N_\downarrow) / N$, and trial wave function. Later, we examine results for other physical quantities such as pairing correlation functions.

A. Ground-state energy

In Fig. 1 we demonstrate the convergence and stability of the CPMC method. The energy (top) and overlap integral

(bottom) are plotted as a function of imaginary time $\tau \equiv n \Delta \tau$. On the left, we demonstrate the initial convergence from the trial wave function to the ground state and, on the right, the asymptotic stability of the algorithm. This figure is constructed for an 8×8 lattice with $\langle n \rangle = 0.875$ and $U = 4$. This parametrization generates a fairly difficult system for the AFQMC method because of the sign problem. $|\Psi_T\rangle$ was an unrestricted Hartree-Fock wave function obtained with $U = 0.4$ (not 4) and yielded a variational energy of -53.05 . The average number of walkers was 600. The behavior shown is quite typical of CPMC calculations.

In the relaxation phase ($\tau \leq 10$), a trial energy of $E_T = -58.0$ was used. This value is significantly higher than the true ground-state energy, and so the overlap integral $\langle \psi_T | \psi^{(n)} \rangle$ and, consequently, the population size grow quite rapidly. During this phase, population control is applied frequently (every five steps). The rapid fluctuations in value of the overlap integral shown in the bottom left are due to readjustments of the total population size in each of these applications. For $10 < \tau \leq 20$ (not shown), we used the same E_T and applied population control with the same frequency, but computed the ground-state energy with the growth estimator. This value was then used for the trial energy E_T during the measurement phase ($\tau > 20$). In this phase, even though population control was applied every ten steps and branching occurs, the total population size remained within the preset lower and upper bounds of 300 and 1200. Indeed, all vertical displacements in the overlap integral in the lower right of the figure correspond to the beginning of a block where we reset the population size to within 10% of the expected average of 600.

Clearly, the values of both the overlap integral and the energy are completely stable as a function of n . In contrast, the standard AFQMC method has a bad sign problem. Indeed, for a 4×4 lattice at the same filling fraction and the same U , the average sign decays exponentially by roughly 5 orders of magnitude as the imaginary time τ increases from 0 to 20.¹

The ground-state energy $E_0^c = -65.135 \pm 0.008$. (Extrapolation to $\Delta \tau = 0$ will slightly reduce the average value.) The best AFQMC result available for this system is -65.02 ± 0.06 ,²⁹ which is slightly higher than our upper bound. The τ dependence of the energy after convergence is shown in the upper right of the figure. The inset demonstrates the short-term fluctuations in the mixed estimate of the energy; these fluctuations are also shown as the solid line in the main figure. Constructing local ‘‘binned’’ averages of the energy from blocks of length $\tau = 10$ yields the energy estimates shown as dotted lines in the inset. These binned averages are nearly statistically independent, and their root-mean-squared deviations divided by the square root of the number of bins yielded the quoted statistical error.

The computational requirements of the CPMC method are fairly modest when compared, for example, with the AFQMC method. Efficiency, however, can be dramatically affected by implementation issues. Two important issues are the accuracy of the trial wave function and of the imaginary-time propagator. To obtain the maximum efficiency, it is essential to use a propagator accurate to second order in the breakup between kinetic and potential terms. For example, Fig. 2 shows the energies obtained for first-order and second-

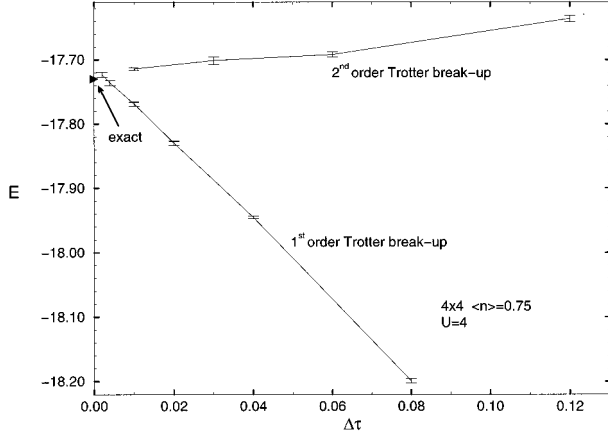


FIG. 2. Illustration of the Trotter approximation error. The computed energy per site is shown as a function of the time step $\Delta\tau$ for a 4×4 lattice with $6 \uparrow 6 \downarrow$ electrons and $U=4$. The first-order Trotter approximation leads to significant finite time-step error. With the second-order approximation, convergence to the $\Delta\tau=0$ limit is much more rapid. The right triangle indicates the exact energy for this system. The variational nature of the CPMC energies is visible. The Monte Carlo error bars are indicated. Curves are to aid the eye.

order Trotter approximations for the propagators for a 4×4 lattice with $N_{\uparrow}=N_{\downarrow}=6$ spins and $U=4$. The first-order propagator introduces significant systematic effects even for quite small time steps; however, the second order propagator permits significantly larger values of $\Delta\tau$ to be used. We note that we also included a mirror correction to the propagation to make certain that there are no corrections of order less than $(\Delta\tau)^2$. In this case, however, the differences between using second-order propagators with and without this correction are comparable to the error bars in the figure.

Of course, while stability and efficiency are necessary for a useful simulation, accuracy is the principal concern. In Tables I and II, we compare our results for the Hubbard model to exact results for small systems and to other methods for large systems. Since the CPMC method depends upon approximate knowledge of the ground state of the system, we also included results for different trial wave functions. To date, we have used only free-electron and unrestricted Hartree-Fock (UHF) trial wave functions.

In Table I, we see that the accuracy of the CPMC ground-state energy is always better than 5%, often much better, even when the trial wave function is very poor. The worst case is 3×3 with 4 \uparrow and 4 \downarrow spins, which is an open-shell case that corresponds to a very difficult filling fraction for the AFQMC method, and has a large U of 8, which makes single-determinant trial wave functions rather poor approximations. The Hartree-Fock wave function used as $|\psi_T\rangle$ had a very poor energy, -0.0025 , compared to the exact energy of -0.809 . The CPMC method, however, was still able to obtain an energy of $-0.766(2)$. Clearly a more accurate approximation to the ground-state wave function would yield an even better result.

In Table II we compare our results with available data from other numerical approaches, including stochastic diagonalization (SD),³² AFQMC, and density-matrix renormalization group (DMRG) (Ref. 33) methods. The SD method uses Monte Carlo methods to attempt the construction of an effi-

TABLE I. Hubbard-model ground-state energies per site from CPMC simulations compared with exact results. The first column under “system” is the lattice size and, the second, the numbers of electrons with \uparrow and \downarrow spins. U is the on-site Coulomb repulsion. The trial wave function $|\psi_T\rangle$ used in CPMC is either a free-electron (free) or an unrestricted Hartree-Fock (UHF) wave function. E_{var} indicates the corresponding variational energy from this wave function. Statistical errors are in the last digit and are shown in parentheses. Exact results for the 4×4 systems are taken from Refs. 30–32.

System	U	$ \psi_T\rangle$	E_{var}/N	E_{CPMC}/N	E_{exact}/N
2×2 $2 \uparrow 1 \downarrow$	4	UHF	-1.5327	-1.6038(6)	-1.6046
2×3 $2 \uparrow 2 \downarrow$	4	free	-1.267	-1.3828(9)	-1.4009
2×3 $2 \uparrow 2 \downarrow$	8	free	-0.889	-1.221(2)	-1.244
2×4 $2 \uparrow 2 \downarrow$	4	UHF	-1.333	-1.3678(5)	-1.374
2×4 $3 \uparrow 3 \downarrow$	4	UHF	-1.438	-1.5693(5)	-1.569
1×8 $3 \uparrow 3 \downarrow$	4	free	-0.645	-0.8329(7)	-0.834
3×3 $4 \uparrow 4 \downarrow$	8	UHF	-0.0025	-0.766(2)	-0.809
4×4 $2 \uparrow 2 \downarrow$	4	UHF	-2.8225	-2.8813(3)	-2.8825
4×4 $4 \uparrow 4 \downarrow$	4	UHF	-1.025	-1.095(1)	-1.096
4×4 $5 \uparrow 5 \downarrow$	8	free	-0.7188	-1.0925(7)	-1.0944
4×4 $6 \uparrow 6 \downarrow$	4	UHF	-1.3117	-1.4763(5)	-1.478
4×4 $7 \uparrow 7 \downarrow$	4	UHF	-0.8669	-0.9831(6)	-0.9838
4×4 $7 \uparrow 7 \downarrow$	12	UHF	-0.474	-0.606(5)	-0.628

cient basis for approximating the ground-state wave function of the system. Since an explicit basis is used, no sign problem occurs; however, an exponential growth in computing time occurs, reflecting the increased effort in selecting members of the basis as system size increases. In contrast, the AFQMC method is in principle exact, but suffers from exponential growth in computing time as the system size increases because of the sign problem. Finally, the DMRG method is a variational method that is very effective for one-dimensional and quasi-one-dimensional models.

TABLE II. Hubbard-model ground-state energies from CPMC simulations compared with available results from other approaches. The first two columns follow the same convention as the corresponding ones in Table I. The interaction strength U is 4. The stochastic diagonalization (SD) results are from Ref. 32; the density-matrix renormalization group (DMRG) results on two chains are from Ref. 34. The statistical errors are in the last one or two digits, as indicated.

System	$ \psi_T\rangle$	E_{CPMC}	E_{SD}	E_{AFQMC}
4×4 $5 \uparrow 5 \downarrow$	free	-19.582(5)	-19.58	-19.58(1)
6×6 $13 \uparrow 13 \downarrow$	free	-42.34(2)	-40.77	-42.32(7)
6×6 $14 \uparrow 14 \downarrow$	UHF	-40.17(2)		-40.44(22)
8×8 $25 \uparrow 25 \downarrow$	free	-72.48(2)	-67.00	-72.80(6)
8×8 $27 \uparrow 27 \downarrow$	UHF	-67.46(4)		-67.55(19)
10×10 $41 \uparrow 41 \downarrow$	free	-109.55(3)		-109.7(6)
12×12 $61 \uparrow 61 \downarrow$	free	-153.43(5)		-151.4(1.4)
16×16 $101 \uparrow 101 \downarrow$	free	-286.55(8)		
System	$ \psi_T\rangle$	E_{CPMC}	E_{DMRG}	
2×8 $7 \uparrow 7 \downarrow$	free	-13.067(4)	-13.0664(2)	
2×16 $14 \uparrow 14 \downarrow$	free	-26.87(2)	-26.867(3)	

TABLE III. Comparisons of the computed expectation values and correlation functions by different estimators for a 4×4 lattice with $5 \uparrow 5 \downarrow$ electrons and $U=4$. The trial wave function is the free-electron wave function. The corresponding variational values from it are shown in the first row. The next row contains mixed estimates from CPMC simulations, while ‘‘Extrap’’ shows the values extrapolated from the first two rows via Eq. (33). The row labeled BP gives the CPMC result via the back-propagation scheme. In the last row, D_{1s} is from AFQMC simulations (Ref. 32), while the others are exact diagonalization results, with the first four from Ref. 30 and the last from Ref. 35. E_k indicates the kinetic energy, $\rho(l_x, l_y)$ the one-body density matrix, S and S_d the spin and charge density structure factors, and D_{1s} and D_{2d} the s - (on-site) and d -wave pairing correlations, respectively. The Monte Carlo errors are shown in parentheses.

	E_k	$\rho(2,1)$	$S(\pi, \pi)$	$S_d(\pi, \pi)$	$D_{1s}(2,1)$	$D_{2d}(2,1)$
Variational	-24.0	-0.0625	0.625	0.625	0.003906	0.03125
Mixed	-24.0(0)	-0.0625(0)	0.6938(4)	0.5572(1)	0.000684(3)	0.03095(2)
Extrap	-24.0(0)	-0.0625(0)	0.763(1)	0.4894(2)	-0.002538(6)	0.03065(4)
BP	-22.55(2)	-0.0563(3)	0.729(1)	0.508(1)	-0.000615(9)	0.0246(2)
Exact	-22.52	-0.0560	0.73	0.506	-0.00058(5)	0.02453

In Table II we focus on filling fractions $\langle n \rangle$ around or greater than 80% as they are more interesting and also more difficult for QMC calculations. For the closed-shell 4×4 system, the results from the CPMC, SD, and AFQMC methods agree well. As we increase the lattice size, the SD results are comparatively poorer, presumably because of an insufficient number of states. The results from the AFQMC and CPMC methods continue to agree well up to fairly large lattice sizes. The worst case is an 8×8 lattice with 25 \uparrow and 25 \downarrow spins, where the CPMC result lies approximately $0.4\% \pm 0.2\%$ above the AFQMC result. For still larger lattice sizes, the sign problem limits the use of the AFQMC method to only closed-shell systems, for which the sign problem is much reduced. Even in these cases, we see that the error estimates in AFQMC are much larger than the corresponding statistical errors from the CPMC method. In the 12×12 case, the difference is roughly a factor of 30, i.e., about a factor of 900 more in CPU time. (Our calculations typically took tens of hours on an IBM RS6000 590.) Furthermore, the CPMC result is actually lower in energy in this case than the AFQMC results, but size of the error bars in AFQMC is similar to the difference between the two results. The CPMC result on a 16×16 lattice, a size far beyond the reach of the AFQMC method due to the sign problem, was obtained from a simulation comparable to that for the 12×12 system in terms of the numbers of iterations and walkers. For the two-chain system, we obtained excellent agreement with the DMRG results of Noack.³⁴ Here the energy agreed to within less than 0.1%.

B. Correlation functions

To effectively study ground-state properties, we need to accurately calculate pairing correlation functions, momentum distributions, and other ground-state expectation values. In previous sections, we discussed various ways of estimating a ground-state expectation value, in particular the back-propagation scheme. Here we will mostly benchmark results and further discuss related algorithmic behavior. We remark that for any simulation method correlation functions are in general much more difficult to compute than the energy. Thus there is limited data available from other methods with which we can benchmark our correlation functions. This

means that self-consistency checks (e.g., comparison of results obtained with different choices of $|\psi_T\rangle$) are crucial.

In Table III, we show results on the simple closed-shell 4×4 system of $5 \uparrow 5 \downarrow$ electrons at $U=4$ and with $\Delta\tau=0.05$. The one-body density matrix is the expectation value of the Green’s function elements: $\rho(\mathbf{I}) = \langle c_0^\dagger c_1 \rangle$, where $\mathbf{I} = (l_x, l_y)$. The spin density structure factor is

$$S(k_x, k_y) = S(\mathbf{k}) = 1/N \sum_{\mathbf{l}} \exp(i\mathbf{k} \cdot \mathbf{l}) \langle \mathbf{s}_0 \mathbf{s}_l \rangle, \quad (46)$$

where $\mathbf{s}_l = n_{l\uparrow} - n_{l\downarrow}$ is the spin at site \mathbf{l} . The charge density structure factor S_d is similar to Eq. (46), with spin replaced by density, i.e., with the $-$ sign in \mathbf{s}_l replaced by a $+$ sign. The electron pairing correlation is defined as

$$D_\alpha(l_x, l_y) = D(\mathbf{I}) = \langle \Delta_\alpha^\dagger(\mathbf{I}) \Delta_\alpha(\mathbf{0}) \rangle, \quad (47)$$

where α indicates the nature of pairing. The on-site s -wave pairing function has $\Delta_{1s}(\mathbf{I}) = c_{l\uparrow} c_{l\downarrow}$, while in this particular case for d -wave pairing we used $\Delta_{2d}(\mathbf{I}) = c_{l\uparrow} \sum_{\delta} f(\delta) c_{l+\delta\downarrow}$, where δ is $(\pm 1, 0)$ and $(0, \pm 1)$. For δ along the x axis, $f(\delta)$ is 1; otherwise, it is -1 . We average over different $\mathbf{0}$ sites to improve statistics.

In Table III we compare CPMC results from the back propagation estimate with exact results. (The length of back-propagation was $\tau=6$.) We see that the CPMC result is essentially exact for this system. The variational results suggest that the free-electron function $|\psi_T\rangle$ is not a very good trial wave function. Nonetheless, the constrained path error seems to be negligibly small. In fact, very limited branching occurs in the calculations, which indicates effective importance sampling with $|\psi_T\rangle$. Furthermore, as U is increased to 8, the variational results become worse, but the CPMC results obtained with the same $|\psi_T\rangle$ remain accurate.⁶ Also in this table are estimates by the mixed and extrapolation schemes discussed in Sec. III C. While these schemes often improve the variational results considerably, their systematic errors are significant, particularly when compared to the high level of statistical accuracy that can be achieved with the CPMC method.

In Table IV, we show expectation values for a system of $7 \uparrow 7 \downarrow$ electrons. This open-shell case has the worst sign

TABLE IV. Computed expectation values and correlation functions from CPMC for a 4×4 lattice with $7\uparrow 7\downarrow$ electrons and $U=4$, compared with exact results. Results are shown for two different trial wave functions $|\psi_{T1}\rangle$ and $|\psi_{T2}\rangle$. Exact diagonalization results are from Ref. 30; numbers in parentheses indicate either the range of values due to the ground-state degeneracy or uncertainties in extracting numbers from a graph. Statistical errors on the last digit of the CPMC results are in parentheses. Symbols are the same as in Table III. n_k is momentum distribution.

	E_k	$\rho(1,0)$	$\rho(2,2)$	$S(\pi, \pi)$	$S_d(\pi, \pi)$	$n_k(\pi/2, 0)$
Variational $ \psi_{T1}\rangle$	-24.0	0.1875	-0.0625	1.654	0.625	1.0
$ \psi_{T2}\rangle$	-21.88	0.1706	-0.0602	4.39	0.516	0.941
CPMC $ \psi_{T1}\rangle$	-21.44(2)	0.168(1)	-0.051(1)	2.90(1)	0.432(1)	0.92(1)
$ \psi_{T2}\rangle$	-21.39(8)	0.168(1)	-0.049(1)	2.92(2)	0.430(1)	0.92(1)
Exact	-21.39(1)	0.168(1)	-0.051	2.16(2)	0.425	0.93(1)

problem for a 4×4 system. We show results from CPMC simulations with two different trial wave functions. Both are unrestricted Hartree-Fock wave functions, but $|\psi_{T1}\rangle$ was obtained with a U of 0.1, while $|\psi_{T2}\rangle$ with $U=4$. The calculation with $|\psi_{T1}\rangle$ has much less fluctuation, even though $|\psi_{T2}\rangle$ has a lower variational energy. In fact, we found this trend to be rather general: Free-electron-like wave functions tend to be better importance functions than unrestricted Hartree-Fock wave functions. We see that the two trial wave functions yield very different variational estimates, but their CPMC results are consistent and in reasonable agreement with exact results. For example, in the free-electron-like function $|\psi_{T1}\rangle$, the momentum distribution is a step function, and the $\mathbf{k}=(1,0)$ state is completely occupied ($n_k=1$), but even with this trial wave function the CPMC method still gives the correct occupation of 0.92(1).

In Fig. 3 we show the d -wave pairing correlation function $D_{2d}(\mathbf{l})$ and static magnetic structure factor $S(\mathbf{k})$. Our general definition of $\Delta_{2d}(\mathbf{l})$ for Eq. (47) is slightly different from the 4×4 case mentioned above. It is $\Delta_{2d}(\mathbf{l}) = \sum_{\delta} \delta^{\mathbf{l}} (c_{1\uparrow} c_{1+\delta} - c_{1\downarrow} c_{1+\delta})$. We show results obtained with two different trial wave functions for a 6×6 system. The expectation values obtained directly from these two different trial wave functions are shown as thick lines, and the corresponding back-propagation estimates $\langle \mathcal{O} \rangle_{BP}$ are shown as thin lines. While the two CPMC estimates do not agree exactly, they do demonstrate a much closer correspondence with each other than those obtained with the original wave functions. The case shown is comparatively easy because of the small size of the lattice and the relatively low value of electron filling. However, the overall trend is rather general.

VI. SUMMARY AND DISCUSSION

We described in detail the background, formalism, and implementation of a constrained path Monte Carlo algorithm. The CPMC method is a general quantum Monte Carlo algorithm for computing fermion ground-state properties. It introduces several new concepts, including importance-sampled random walks in a Slater-determinant space and the constrained path approximation within this framework. The algorithm combines advantages of the existing Green's function Monte Carlo and auxiliary-field quantum Monte Carlo methods, is free of any signal-to-noise ratio decay, and scales algebraically with system size. Together with data in Ref. 6, we demonstrated that the method produces very accurate re-

sults for the Hubbard model, even with very simple choices of the trial wave function $|\psi_T\rangle$.

Compared to the GFMC method, the current algorithm allows the random walk to take place in a basis other than that of configurations or occupation numbers. In this sense, the CPMC algorithm is a generalization of the GFMC algorithm. The CPMC method expresses the ground-state wave function (stochastically) in the form of Eq. (20), rather than $\psi_0(R) = \sum_k \delta(R - R_k)$ as in the GFMC method. This form is advantageous as it makes feasible the use of various techniques developed for one-electron calculations for atoms and solids. In addition, it makes our back-propagation scheme efficient and effective. Thus expectation values can be computed via Eq. (7), while in the GFMC method the analogous forward-walking technique has often been difficult and computations of some correlation functions have almost been impossible. If applications of the CPMC method to continuum systems are successful, the ability to compute the

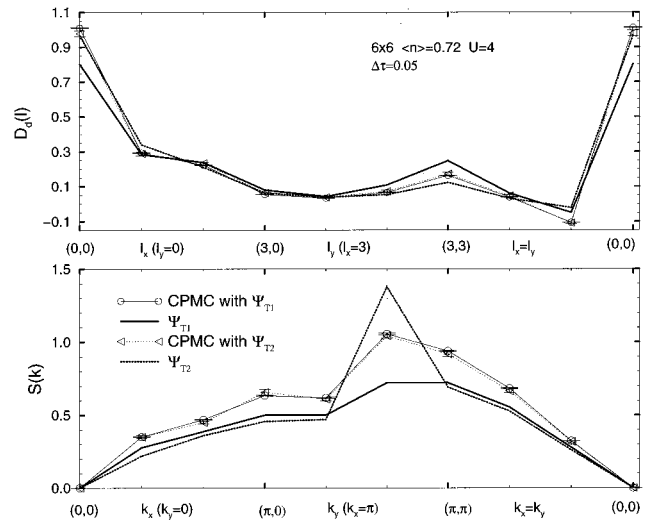


FIG. 3. Sensitivity of CPMC results to the choice of trial wave function $|\Psi_T\rangle$ for some correlation functions. The upper figure is the d -wave electron pairing correlation $D_{2d}(\mathbf{l})$ and the lower curve is the magnetic structure factor $S(\mathbf{k})$. The free-electron wave function $|\psi_{T1}\rangle$ and the unrestricted Hartree-Fock wave function $|\psi_{T2}\rangle$ (with $U=4$) are used. The corresponding mean-field results for these correlation functions are also shown (thick lines). The computed ground-state energies from CPMC are $-42.345(3)$ and $-42.295(16)$ (cf. Table II).

expectation values of such quantities as forces will be very valuable. These applications are under study.

There is an obvious resemblance between the constrained path (CP) approximation in the CPMC method and the fixed-node (FN) approximation in the GFMC method. Both result in solutions to the Schrödinger equation that are consistent with some artificial boundary conditions. An important difference, however, is also evident. The FN approximation is in configuration space and requires the solution to have a predefined node: $\psi_0^{\text{FN}}(R)=0$ where $\psi_T(R)=0$. The CPMC method is in a Slater-determinant space. The CP approximation on each individual Slater determinant $|\phi\rangle$, translated into configuration space $|R\rangle$, is nonlocal and requires $\int \psi_T(R)\phi(R)dR > 0$. Thus the node, as well as the amplitude $\phi(R)$, is allowed to vary. The systematic error in the CPMC method arises because the solution it yields, in the form of Eq. (18), has the artificial constraint $\chi_{\psi_0}(\phi) > 0$.

In the CPMC method, each Slater determinant $|\phi\rangle$ analytically defines a continuous function $\phi(R)$ in contrast to walkers in the GFMC method which are δ functions. It is thus easier to impose symmetries. One example is the trivial case of a noninteracting system: The CPMC method naturally yields the correct result, while standard GFMC still requires knowledge of the node. Another is the one-band Hubbard model at half-filling, where the CPMC method retains the exact nature of the AFQMC method, while the GFMC method retains the sign problem.³⁶

Recently, ten Haaf and van Leeuwen³⁷ presented data on the Hubbard model from standard GFMC simulations with the fixed-node approximation, which they and collaborators had earlier generalized³⁸ to treat lattice fermion systems. For the 4×4 system in Table II ($5 \uparrow 5 \downarrow U=4$), the CPMC result for the energy per site is $E/N = -1.2239(3)$ (exact value³⁰) of -1.2238). With an *identical* trial wave function, the fixed-node calculations of ten Haaf and van Leeuwen yielded $-1.2186(4)$. Incorporating a Gutzwiller factor only slightly improved their FN result to $-1.2201(4)$. Unfortunately, the rest of their results are all FN energies computed for half-filled systems, for which the CPMC energies would be *exact*. Further comparisons away from half-filling would allow a more systematic understanding of the relative strengths of the CPMC method.

It is worth noting that the CPMC algorithm provides a stochastic method closely linked with more traditional quantum chemistry approaches such the configuration interaction (CI) method. Similar to the CI method, the CPMC method produces a collection of determinants whose sum represents the ground-state wave function. The determinants, however, do not have to be orthogonal to each other. Furthermore, they are generated efficiently and *systematically* by a Monte

Carlo process that is *guided* by importance sampling. The drawback of the CPMC method is of course its variational nature due to the CP approximation.

We are currently investigating several schemes for further improving the algorithm. These include a method analogous to released-node technique¹⁶ in the GFMC method. For the energy, this seems straightforward. For other expectation values, it involves evaluating $\langle \mathcal{O} \rangle_{\text{BP}}(\tau_1, \tau_2)$ defined as

$$\begin{aligned} \langle \mathcal{O} \rangle_{\text{BP}}(\tau_1, \tau_2) = & \langle \psi_T \exp[-\tau_2 H^c] \exp[-\tau_1 H] | \mathcal{O} | \\ & \times \exp[-\tau_1 H] | \psi_0 \rangle. \end{aligned} \quad (48)$$

In this expression H is the original Hamiltonian without the constraint, and H^c indicates the Hamiltonian in the presence of the constraint. Hence, for a period of twice τ_1 , we evolve the system without constraint and for another τ_2 we include the constraint. In the limit of zero τ_1 we obtain the approximation used to date, while finite τ_1 improves the estimate, i.e., makes it exact, at the cost of increasing statistical error. The bookkeeping in such a calculation could be arranged to calculate directly the difference between the current $\langle \mathcal{O} \rangle_{\text{BP}}$ and the transient estimation and, hence, to provide a stringent test on the accuracy of a given calculation.

Other possibilities for improving estimates of expectation values include optimization techniques for improving the trial wave function. As mentioned earlier, the algorithm as described can be used with a multideterminant $|\psi_T\rangle$, with the computational cost increasing only linearly with the number of determinants. Thus it is desirable to have good trial wave functions in the form of linear combinations of Slater determinants. In addition, wave functions in this form that can be tuned systematically to yield different properties would be highly useful, since self-consistency checks with the CPMC method can then be carried out simply by changing parameters in $|\psi_T\rangle$. Yet other algorithmic topics include the development of interacting-walker²¹ and mirror potential³⁹ analogs.

ACKNOWLEDGMENTS

We thank A. Moreo, R. M. Noack, and R. T. Scalettar for providing unpublished data, M. H. Kalos, D. J. Scalapino, and C. J. Umrigar for stimulating discussions, and M. Guerro, M. M. Steiner, and J. W. Wilkins for helpful comments on the manuscript. This work was supported in part by the Applied Mathematics Program of the Department of Energy. Calculations were performed at the Cornell Theory Center on the SP2 computer. S.Z. also acknowledges support by DOE-BES, Division of Material Science (Grant No. DE-FG02-88ER45347).

*Present address: Department of Physics and Department of Applied Physics, College of William and Mary, Williamsburg, VA 23187.

¹E. Y. Loh, Jr., J. E. Gubernatis, R. T. Scalettar, S. R. White, D. J. Scalapino, and R. L. Sugar, Phys. Rev. B **41**, 9301 (1990).

²K. E. Schmidt and M. H. Kalos, in *Applications of the Monte Carlo Method in Statistical Physics*, edited by K. Binder (Springer-Verlag, Heidelberg, 1984).

³D. M. Ceperley and M. H. Kalos, in *Monte Carlo Methods in*

Statistical Physics, edited by K. Binder (Springer-Verlag, Heidelberg, 1979).

⁴D. M. Ceperley, Rev. Mod. Phys. **67**, 279 (1995).

⁵For a survey of quantum Monte Carlo methods for lattice problems, see H. De Raedt and W. von der Linden, in *The Monte Carlo Method in Condensed Matter Physics*, edited by K. Binder (Springer-Verlag, Heidelberg, 1992).

⁶Shiwei Zhang, J. Carlson, and J. E. Gubernatis, Phys. Rev. Lett. **74**, 3652 (1995).

- ⁷M. H. Kalos, D. Levesque, and L. Verlet, *Phys. Rev. A* **9**, 2178 (1974).
- ⁸We will use the phrase “Green’s function Monte Carlo” in a very general sense to indicate methods that project the ground state from a trial initial state by an importance-sampled random walk, where wave functions are expressed in a configuration basis and represented by a Monte Carlo sample. The difference in the methods will be attributed to differences in the choice of the projection operator.
- ⁹R. Blankenbecler, D. J. Scalapino, and R. L. Sugar, *Phys. Rev. D* **24**, 2278 (1981).
- ¹⁰G. Sugiyama and S. E. Koonin, *Ann. Phys. (N.Y.)* **168**, 1 (1986).
- ¹¹See E. Y. Loh, Jr. and J. E. Gubernatis, in *Electrons Phase Transitions*, edited by W. Hanke and Y. V. Kopaev (Elsevier, New York, 1990), and references therein.
- ¹²We will use the phrase “auxiliary-field quantum Monte Carlo” to refer to the class of fermion methods briefly summarized in Sec. II A. We note that the adoption of this name is relatively recent, even though the methods have been used for a number of years, often with the generic name quantum Monte Carlo, both at finite and zero temperatures. Here we use “AFQMC” in order to distinguish from other QMC methods.
- ¹³S. B. Fahy and D. R. Hamann, *Phys. Rev. Lett.* **65**, 3437 (1990); *Phys. Rev. B* **43**, 765 (1991).
- ¹⁴J. B. Anderson, *J. Chem. Phys.* **63**, 1499 (1975); **65**, 4122 (1976).
- ¹⁵J. W. Moskowitz, K. E. Schmidt, M. A. Lee, and M. H. Kalos, *J. Chem. Phys.* **77**, 349 (1982); P. J. Reynolds, D. M. Ceperley, B. J. Alder, and W. A. Lester, *ibid.* **77**, 5593 (1982).
- ¹⁶D. M. Ceperley and B. J. Alder, *Phys. Rev. Lett.* **45**, 566 (1980); *J. Chem. Phys.* **81**, 5833 (1984).
- ¹⁷S. R. White, D. J. Scalapino, R. L. Sugar, E. Y. Loh, Jr., J. E. Gubernatis, and R. T. Scalettar, *Phys. Rev. B* **40**, 506 (1989).
- ¹⁸M. H. Kalos, *J. Comput. Phys.* **2**, 257 (1967).
- ¹⁹J. W. Negele and H. Orland, *Quantum Many-Particle Systems* (Addison-Wesley, New York, 1987), Chap. 7.
- ²⁰For a review of the DMC method, see B. L. Hammond, W. A. Lester, Jr., and P. J. Reynolds, *Monte Carlo Methods in Ab Initio Quantum Chemistry* (World Scientific, Singapore, 1994).
- ²¹Shiwei Zhang and M. H. Kalos, *Phys. Rev. Lett.* **67**, 3074 (1991); J. B. Anderson, C. A. Traynor, and B. M. Boghosian, *J. Chem. Phys.* **95**, 7418 (1991).
- ²²Zhiping Liu, Shiwei Zhang, and M. H. Kalos, *Phys. Rev. E* **50**, 3220 (1994); M. H. Kalos (unpublished).
- ²³If $|\psi_T\rangle$ is a linear combination of Slater determinants, we can initialize walkers by sampling the individual Slater determinants according to their overlap with $|\psi_T\rangle$. Ones with negative overlaps are either avoided or manipulated so that the form used in the initial population gives a positive overlap.
- ²⁴Shiwei Zhang, J. Carlson, and J. E. Gubernatis (unpublished).
- ²⁵J. E. Hirsch, *Phys. Rev. B* **31**, 4403 (1985).
- ²⁶We recently observed that in one dimension we can make our method exact for several broad classes of problems. For these classes, the dimensionality, boundary conditions, and electron density fixes the location of the nodal points of the exact many-electron wave function at places identical to those of simply constructed approximate wave functions. We will discuss this development more fully elsewhere.
- ²⁷One can attempt to improve the calculation of $\langle \mathcal{O} \rangle^c$ by creating a better importance sampling for the left-hand random walk that both imposes the constraint with $|\psi_T\rangle$ and attempts to incorporate the necessary correlations between the left-hand random walker and its matching right-hand walker. For example, we can take an importance function $O_T^L(\phi') = |\langle \phi' | \phi_k^{(n)} \rangle| + \alpha \langle \phi' | \psi_T \rangle$, where α is a parameter and $|\phi_k^{(n)}\rangle$ is the walker with which ϕ' will be matched in the regular population representing the right-hand wave function. While this offers a significant improvement over the naive calculation of $\langle \mathcal{O} \rangle^c$, we found it still prone to significant fluctuations. We are investigating other schemes to provide more accurate calculations of the direct expectation value.
- ²⁸J. H. Hetherington, *Phys. Rev. A* **30**, 2713 (1984).
- ²⁹N. Furukawa and M. Imada, *J. Phys. Soc. Jpn.* **61**, 3331 (1992).
- ³⁰A. Parola, S. Sorella, S. Baroni, R. Car, M. Parrinello, and E. Tosatti, *Physica C* **162-164**, 771 (1989); A. Parola, S. Sorella, M. Parrinello, and E. Tosatti, *Phys. Rev. B* **43**, 6190 (1991).
- ³¹G. Fano, F. Ortolani, and A. Parola, *Phys. Rev. B* **42**, 6877 (1990).
- ³²H. De Raedt and M. Frick, *Phys. Rep.* **231**, 109 (1993).
- ³³S. R. White, *Phys. Rev. Lett.* **69**, 2863 (1992); *Phys. Rev. B* **48**, 10 345 (1993).
- ³⁴R. M. Noack (private communication).
- ³⁵A. Moreo (private communication).
- ³⁶Care must be taken in constructing the importance function in the half-filled case. The definition in Eq. (22) introduces an artificial “node” $\langle \psi_T | \phi \rangle = 0$. As $\Delta\tau \rightarrow 0$, this prevents walkers from tunneling and incorrectly confines the random walk. To remedy this, we use several determinants: $O_T(\phi) = \sum_j |\langle \psi_T^j | \phi \rangle|$. An alternative would be to shift O_T by a constant.
- ³⁷D. F. B. ten Haaf and J. M. J. van Leeuwen (unpublished).
- ³⁸D. F. B. ten Haaf, H. J. M. van Bommel, J. M. J. van Leeuwen, W. van Saarloos, and D. M. Ceperley, *Phys. Rev. B* **51**, 13 039 (1995); H. J. M. van Bommel, D. F. B. ten Haaf, W. van Saarloos, J. M. J. van Leeuwen, and G. An, *Phys. Rev. Lett.* **72**, 2442 (1994).
- ³⁹J. Carlson and M. H. Kalos, *Phys. Rev. C* **32**, 1735 (1985); R. M. Panoff and J. Carlson, *Phys. Rev. Lett.* **62**, 1130 (1989).